

Surface-bulk coupling in a Bi_2Te_3 nanoplate grown by van der Waals epitaxy

Xiaobo Li^{1,2}, Mengmeng Meng¹, Shaoyun Huang¹, Congwei Tan³, Congcong Zhang³, Hailin Peng³, and H. Q. Xu^{1,4,*}

¹*Beijing Key Laboratory of Quantum Devices, Key Laboratory for the Physics and Chemistry of Nanodevices, and School of Electronics, Peking University, Beijing 100871, China*

²*Academy for Advanced Interdisciplinary Studies, Peking University, Beijing 100871, China*

³*Center for Nanochemistry, Beijing National Laboratory for Molecular Sciences (BNLMS), College of Chemistry and Molecular Engineering, Peking University, Beijing 100871, China*

⁴*Beijing Academy of Quantum Information Sciences, Beijing 100193, China*

*Corresponding authors: H. Q. Xu (hqxu@pku.edu.cn)

(Date: January 19, 2022)

ABSTRACT

We report on an experimental study of the effect of coherent surface-bulk electron scattering on quantum transport in a three-dimensional topological insulator Bi_2Te_3 nanoplate. The nanoplate is grown via van der Waals epitaxy on a mica substrate and a top-gated Hall-bar device is fabricated from the nanoplate directly on the growth substrate. Top-gate voltage dependent measurements of the sheet resistance of the device reveal that the transport carriers in the nanoplate are of n-type and that, with decreasing top gate voltage, the carrier density in the nanoplate is decreased. However, the mobility is increased with decreasing top-gate voltage. This mobility increase with decreasing carrier density in the nanoplate is demonstrated to arise from a decrease in bulk-to-surface electron scattering rate. Low-field magnetotransport measurements are performed at low temperatures. The measured magnetoconductivity of the nanoplate shows typical weak anti-localization (WAL) characteristics. We analyze the measurements by taking surface-bulk inter-channel electron scattering into account and extract dephasing times τ_φ , diffusion coefficients D of electrons at the top surface and in the bulk, and the surface-bulk scattering times τ_{SB} as a function of top-gate voltage and temperature. It is found that the dephasing in the nanoplate arises dominantly from electron-electron scattering with small energy transfers. It is also found that the ratio of $\tau_\varphi/\tau_{\text{SB}}$ (a measure of the surface-bulk electron coherent coupling) is decreased with decreasing gate voltage or increasing temperature. We demonstrate that taking the surface-bulk

coherent electron scattering in our Bi_2Te_3 nanoplate into account is essential to understand quantum transport measurements at low temperatures.

Three-dimensional (3D) topological insulators (TIs) are a new class of quantum materials which possess gapped bulk and gapless surface states.^{1, 2} Due to time-reversal symmetry and spin-momentum interlock, these surface, topological, helical Dirac fermion states are attractive for applications in low energy-dissipative spintronics^{3,4} and for construction of Majorana bound states.⁵ In physics, the helical Dirac fermion quasiparticles at the surface traveling through the coherent time-reversed closed paths can interfere, leading to a positive quantum correction to the conductivity and thus the weak anti-localization (WAL) effect.⁶ In experiments, the detection of topological surface states in 3D TIs is usually carried out through analysis of the WAL effect observed in transport measurements at low magnetic fields.⁷⁻⁹ Unfortunately, due to strong spin-orbit coupling, the conducting bulk state of a 3D TI can also contribute to the WAL effect, which masks the surface signals and thus makes the surface state analysis difficult.^{10,11} To extract the surface state contribution from transport measurements in a 3D TI, one usually carries out the transport measurements of the material at different carrier densities achieved via electrostatic tuning and analyzes the quantum correction to the magnetoconductivity based on the Hikami-Larkin-Nagaoka (HLN) formula.¹²⁻¹⁴ Through fits of the magnetoconductivity to the HLN formula, it has been demonstrated that the extracted absolute value of dimensionless prefactor $|\alpha|$ in the formula (a measure of the number of 2D conduction channels in the material) usually varies from $\sim 1/2$ (surface-bulk state coupled transport in the device) to ~ 1 (transport through separate surface and bulk channels),¹⁵⁻¹⁷ reflecting the existence of the surface states. However, since the effect of the surface-bulk electron scattering is not included in the HLN formula, analysis of the magnetoconductivity based on this formula could make deviations, especially for a case with a strong surface-bulk state coupling. Garate and Glazman have evaluated the quantum correction to magnetoconductivity in a 3D TI film with surface-bulk scattering being taken into consideration.¹⁸ It has been shown that, once states at a surface of a 3D TI film are coupled to the bulk states, the quantum correction to the magnetoconductivity should in general be expressed as a function of dephasing times τ_φ and diffusion coefficients D of carriers at the surface and in the bulk, and surface-bulk inter-channel scattering time τ_{SB} . Using this model to analyze the measured magnetoconductivity, one can extract the transport parameters τ_φ , τ_{SB} and D in a 3D TI film, as well as the ratio of τ_φ/τ_{SB} , i.e., a measure of the strength of the surface-bulk state coupling (with $\tau_\varphi/\tau_{SB} > 1$ referring to the surface-bulk-coherently-coupled case and $\tau_\varphi/\tau_{SB} < 1$ referring to the case where the surface and bulk states are no longer coherently coupled).^{15,19}

Here, we report on a low-temperature transport study of a Bi_2Te_3 nanoplate. The Bi_2Te_3 nanoplate is grown on a mica substrate via van der Waals epitaxy and the transport measurements are made in a top-gated Hall-bar device setup. Top-gate voltage dependent measurements of the sheet resistance of the nanoplate reveal top surface-bulk state coupled, n-type carrier transport characteristics. Low-field magnetotransport measurements are performed for the Bi_2Te_3 nanoplate Hall-bar device at different gate voltages and temperatures. The dephasing times τ_ϕ and the diffusion coefficients D of electrons at the surface and in the bulk, and the surface-bulk electron scattering times τ_{SB} are extracted by fits of the measured magnetoconductivity to the Garate-Glazman theory. It is found that the ratio of $\tau_\phi/\tau_{\text{SB}}$ is gate-voltage and temperature dependent. As the gate voltage decreases or the temperature increases, $\tau_\phi/\tau_{\text{SB}}$ is decreased and thus the strength of the surface-bulk state coupling is weakened.

Bi_2Te_3 nanoplates are grown on a mica substrate with a fresh, cleavage plane via van der Waals epitaxy.²⁰ The inset of Fig. 1(a) shows an optical image of as-grown Bi_2Te_3 nanoplates. These nanoplates have a lateral size of $10 \sim 30 \mu\text{m}$ and a thickness of $4 \sim 20 \text{ nm}$. In fabrication of a Hall-bar device, metal markers are first defined on the growth substrate to locate nanoplates. Then, six electrodes (source, drain and four probe contacts) consisting of 5-nm-thick Ti and 90-nm-thick Au are made on a selected nanoplate by electron-beam lithography for pattern definition, electron-beam evaporation for metal deposition, and lift-off process. After that, a dielectric layer of 20-nm-thick HfO_2 , covering the entire Hall bar and sufficiently large portions of contact electrode, is made by electron-beam lithography, atomic layer deposition and lift-off. Finally, a top gate made of 5-nm-thick Ti and 90-nm-thick Au is fabricated on the HfO_2 dielectric layer again by electron-beam lithography, electron-beam evaporation and lift-off process. Figure 1(a) shows an optical image of a fabricated top-gated Hall-bar device. The device is made from a hexagonal Bi_2Te_3 nanoplate [as marked by the white arrow in the inset of Fig. 1(a)] with a thickness of $\sim 12 \text{ nm}$.

Figure 1(b) shows a schematic diagram of the device structure and the measurement circuit setup. The distance L between probes 1 and 2 or between probes 3 and 4 is designed as $\sim 6 \mu\text{m}$, and the width W of the Hall bar (i.e., the measured distance between probes 1 and 3 or between probes 2 and 4) is designed as $\sim 20 \mu\text{m}$. Cryogenic transport measurements are performed in a physical property measurement system (PPMS) equipped with a superconducting magnet which can provide a magnetic field up to 9 T. In the measurements, both longitudinal voltage V_{xx} and transverse voltage V_{yx} are detected using a standard lock-in technique, in which an ac

current I of 300 nA at a frequency of 17 Hz is supplied between the source and drain contacts. The longitudinal resistance R_{xx} and the Hall resistance R_{yx} are obtained numerically from the measurements as $R_{xx} = \frac{V_{xx}}{I}$ and $R_{yx} = \frac{V_{yx}}{I}$.

Figure 1(c) shows the top-gate voltage dependent measurements of the sheet resistance R (defined as $R = R_{xx} \times \frac{W}{L}$) of the device shown in Fig. 1(a) at $T = 2$ K. It is seen that R increases as the top gate voltage decreases, indicating that the transport carriers in the nanoplate are of electrons. Previously, n-type Bi_2Te_3 layers synthesized by means of van der Waals epitaxy²¹⁻²³ have been reported and the n-type carriers in the materials are thought to be originated from Bi vacancies as well as Te_{Bi} antisites.^{24,25} The blue vertical dashed line in Fig. 1(c) marks the top-gate voltage value of $V_g = 5$ V. As V_g decreases from 10 V to 5 V, the depletion of electrons in the nanoplate causes an increase of R . The sheet resistance R becomes to increase more slowly as the top-gate voltage continues to decrease from $V_g = 5$ V. This could presumably be considered as a result of enhanced screening against the top gate by gradually separated top-surface states. To study the coupling effect between the top surface and bulk states at different carrier densities, we carry out the magnetotransport measurements at $V_g = -10$ V, -3 V, 0 V, 5 V and 11 V. The inset of Fig. 1(c) shows the sheet electron density n , together with the Hall mobility μ , extracted from the measurements. It is found that n decreases as V_g decreases and reaches to a value of $\sim 2.5 \times 10^{14} \text{ cm}^{-2}$ at $V_g = -10$ V. The mobility μ is found to increase as V_g decreases, which implies that transport scattering becomes weakened with decreasing V_g (we will further discuss this important point later). Figure 1(d) shows detailed measurements of the longitudinal resistance R_{xx} and the Hall resistance R_{yx} of the device as a function of the magnetic field B at $T = 2$ K and $V_g = 0$ V. The magnetic field is applied perpendicular to the substrate. The sharp dip seen in the longitudinal resistance R_{xx} in the vicinity of $B = 0$ T reveals a typical WAL effect. The negative slope of the Hall resistance R_{yx} seen in Fig. 1(d) again indicates that the transport carriers in the nanoplate are of electrons.

Figure 2(a) shows the measured magnetoconductivity, $\Delta\sigma_{xx}(B) = \sigma_{xx}(B) - \sigma_{xx}(B = 0)$, at the top-gate voltages selected above and $T = 2$ K (opened circles). Here, σ_{xx} is obtained from $\sigma_{xx} = \frac{R_{xx}}{R_{xx}^2 + R_{yx}^2} \times \frac{L}{W}$ and the measured curves are successively vertically offset for clarify. These magnetoconductivity curves all show typical WAL characteristics. We could analyze these observed WAL characteristics using the Hikami-Larkin-Nagaoka (HLN) formula²⁶ as it

is commonly done in the literature. However, the extracted temperature dependence of the dephasing length from such analyses has been found to deviate strongly from one that would be expected for a 2D system (see Supplementary Materials). Here we are going to analyze our measured WAL characteristics based on a formula derived previously by Garate and Glazman¹⁸, in which the electron transport at the surface and in the bulk, as well as electron scattering between the surface and the bulk states, have been treated explicitly. In the case for our top-gated Bi₂Te₃ nanoplate device, we consider that the top surface and the bulk are the two 2D conduction channels and assume that the bottom surface has a negligible contribution to the 2D WAL effect. This assumption is justified by the fact that it has been hard to observe a contribution to the quantum correction to the conductivity from the bottom surface in a 3D topological insulator grown on a mica substrate^{27,28}, due to the presence of a substantial concentration of defects or stacking faults in the first few layers grown on the mica substrate²⁹. In the view of that the top surface and the bulk of the Bi₂Te₃ nanoplate are the two 2D conduction channels and by considering the electron scattering between the top surface and bulk states, the Garate-Glazman formula for the quantum correction to the magnetoconductivity is given by¹⁸

$$\Delta\sigma_{xx}(B) = \frac{e^2}{2\pi h} \left[f\left(\frac{\hbar q_{\pm}^2}{4eB}\right) + f\left(\frac{\hbar q_{\pm}^2}{4eB}\right) \right], \quad (1)$$

where $f(x) = \ln(x) - \psi(1/2 + x)$, with ψ being the digamma function, and $q_{\pm}^2 = \frac{1}{2} \left(\frac{1}{\tilde{l}_{\varphi_1}^2} + \frac{1}{\tilde{l}_{\varphi_2}^2} \pm \sqrt{\left(\frac{1}{\tilde{l}_{\varphi_1}^2} - \frac{1}{\tilde{l}_{\varphi_2}^2}\right)^2 + \frac{4}{l_{SB_1}^2 l_{SB_2}^2}} \right)$, with $\tilde{l}_{\varphi_i} = \sqrt{D_i \tilde{\tau}_{\varphi_i}}$, $\tilde{\tau}_{\varphi_i}^{-1} = \tau_{\varphi_i}^{-1} + \tau_{SB_i}^{-1}$, $l_{SB_i} = \sqrt{D_i \tau_{SB_i}}$ and $i = 1$ or 2 . Here, τ_{φ_i} and D_i are the dephasing time and diffusion coefficient of electrons in the bulk ($i = 1$) and at the surface ($i = 2$), τ_{SB_1} is the electron scattering time from the bulk to the surface, while τ_{SB_2} is the electron scattering time from the surface to the bulk.

We fit the measured magnetoconductivity data at the different gate voltages to Eq. (1). The dashed lines in Fig. 2(a) show the results of the fits. It is seen that all the measured magnetoconductivity data can be fitted excellently by Eq. (1). Figures 2(b) and 2(c) show the extracted τ_{φ_1} and τ_{φ_2} , τ_{SB_1} and τ_{SB_2} , and D_1 and D_2 from the fits. Comparing dephasing times τ_{φ_1} and τ_{φ_2} , we find that τ_{φ_2} is much longer than τ_{φ_1} at all the selected top-gate voltages. Here, we note that since the top-surface state electrons are topologically protected, it is reasonable to assign τ_{φ_2} to the dephasing time of electrons at the surface. In addition, we find that both τ_{φ_1} and τ_{φ_2} decrease as the top-gate voltage decreases. These gate voltage dependences of τ_{φ_1} and τ_{φ_2} indicate a stronger dephasing process at a lower

top-gate voltage, due to a reduction in Coulomb screening and an enhancement in electron-electron interaction³⁰ at a lower electron density. The bulk-to-surface and surface-to-bulk electron scattering times show different top-gate voltage dependences: τ_{SB_1} increases as the top-gate voltage decreases, while τ_{SB_2} remains nearly unchanged. These results are excellently in agreement with the fact that the surface-to-bulk scattering rate is proportional to the density of states (DOS) in the bulk, i.e., $\tau_{\text{SB}_2}^{-1} \propto \text{DOS}$ in the 2D bulk, which is a constant, while the bulk-to-surface scattering rate is proportional to the DOS at the surface, i.e., $\tau_{\text{SB}_1}^{-1} \propto \text{DOS}$ at the top surface, which increases with increasing Fermi energy (see Supplementary Materials). It is now important to note that the observed increase in the Hall mobility with decreasing gate voltage, as we showed and discussed above, could be attributed to the fact that the inter-2D-channel scattering time τ_{SB_1} of electrons in the bulk is significantly increased as V_g decreases. In addition, τ_{SB_1} is found to be 2.2~3.9 times larger than τ_{SB_2} , which indicates that the bulk possesses a higher DOS than the top surface at the considered values of V_g . The diffusion coefficients extracted for the bulk D_1 and for the top surface D_2 are found to be $D_1 < D_2$ at all these considered top-gate voltages [see the insets in Figs. 2(b) and 2(c)]. It is also seen that both D_1 and D_2 are weakly dependent on V_g [see again the insets in Figs. 2(b) and 2(c)], indicating that the electron diffusion is hardly affected by the electron density at these top-gate voltages. The weak V_g dependences of the diffusion coefficients are consistent with the expectation that $D_1, D_2 \propto E_F \mu$ (see Supplementary Materials) and the observation shown in the inset of Fig. 1(c) that μ increases almost linearly with decreasing V_g (note that, to a good approximation, the Fermi energy E_F can be assumed to decrease linearly with V_g). This result shows again the importance of considering surface-bulk scattering in analyzing the transport properties of the Bi_2Te_3 nanoplate. Figure 2(d) shows the dephasing lengths in the bulk L_{φ_1} and at the top surface L_{φ_2} extracted via $L_{\varphi_1} = \sqrt{D_1 \tau_{\varphi_1}}$ and $L_{\varphi_2} = \sqrt{D_2 \tau_{\varphi_2}}$. As expected, L_{φ_2} exhibits a longer dephasing length than L_{φ_1} and both become smaller at a lower electron density.

To quantify the influence of the top-gate voltage on the strength of the surface-bulk state coupling, we show in Figs. 2(e) and 2(f) the top-gate voltage dependences of $\tau_{\varphi_1}/\tau_{\text{SB}_1}$ and $\tau_{\varphi_2}/\tau_{\text{SB}_2}$. Previously, it was shown that the ratio of $\tau_{\varphi}/\tau_{\text{SB}}$ can be used to characterize the effect of the surface-bulk state coupling.^{15,19} When $\tau_{\varphi}/\tau_{\text{SB}} > 1$, electrons maintain phase coherence during transferring from one 2D conduction channel to the other 2D channel, leading to the formation of a two-channel-coherently-coupled conduction channel, and the system is in

a strong inter-channel coupling case. However, when $\tau_\phi/\tau_{SB} < 1$, electrons will lose phase coherence before being scattered into the other channel and electrons in the two conduction channels are no longer coherently coupled. Figures 2(e) and 2(f) show that both $\tau_{\phi_1}/\tau_{SB_1} > 1$ and $\tau_{\phi_2}/\tau_{SB_2} > 1$ at the considered top-gate voltages. Thus, the electron transport in the Bi_2Te_3 nanoplate is in a surface-bulk coherently coupled case. It is also seen in Figs. 2(e) and 2(f) that $\tau_{\phi_1}/\tau_{SB_1}$ and $\tau_{\phi_2}/\tau_{SB_2}$ decrease with decreasing V_g , reflecting that the strength of the surface-bulk coherent coupling is gradually weakened.

To examine how the transport characteristic parameters in the Bi_2Te_3 nanoplate depend on temperature, we show in Fig. 3(a) the measured magnetoconductivity $\Delta\sigma_{xx}$ (opened circles) at a fixed top-gate voltage of $V_g = -10$ V at different temperatures. Here, again, the measured magnetoconductivity data at different temperatures are successively vertically offset for clarify. It is seen that a WAL magnetoconductivity peak appears in all the considered temperatures but is gradually suppressed with increasing temperature. The measured magnetoconductivity data at different temperatures are fitted to Eq. (1) and the results of the fits are presented by the dashed lines in Fig. 3(a). Figures 3(b) and 3(c) show the characteristic transport parameters τ_{ϕ_1} and τ_{ϕ_2} , τ_{SB_1} and τ_{SB_2} , and D_1 and D_2 extracted from the fits. It is found that τ_{SB_1} , τ_{SB_2} , D_1 and D_2 all are weakly temperature dependent. However, τ_{ϕ_1} and τ_{ϕ_2} are found to be strongly temperature dependent and, as expected, they both decrease with increasing temperature. Figure 3(d) shows dephasing lengths L_{ϕ_1} and L_{ϕ_2} obtained from $L_{\phi_i} = \sqrt{D_i\tau_{\phi_i}}$ with $i = 1$ and 2 . Both L_{ϕ_1} and L_{ϕ_2} are found to exhibit a power-law temperature dependence, $L_{\phi_1} \sim T^{-0.55}$ and $L_{\phi_2} \sim T^{-0.49}$, showing that the electron dephasing both at the top surface and in the bulk arises dominantly from electron-electron scattering with small-energy transfers.³⁰ Figures 3(e) and 3(f) show the temperature dependences of $\tau_{\phi_1}/\tau_{SB_1}$ and $\tau_{\phi_2}/\tau_{SB_2}$. It is seen that both $\tau_{\phi_1}/\tau_{SB_1}$ and $\tau_{\phi_2}/\tau_{SB_2}$ decrease with increasing temperature (i.e., an increase in temperature will weaken the strength of the surface-bulk state coherent coupling due to a decrease in dephasing time). It is important to note that $\tau_{\phi_1}/\tau_{SB_1} < 1$ when $T \geq 6$ K. This indicates that electrons in the bulk would lose phase coherence before being scattered into the top surface at $T \geq 6$ K and thus the coherent electron transport in the bulk could well be treated within the single 2D channel framework. However, $\tau_{\phi_2}/\tau_{SB_2} > 1$ at all considered temperatures, which indicates that the coherent electron transport at the top surface could not be properly treated without considering electron scattering into the bulk at these temperatures.

In conclusion, a top-gated Hall-bar device has been fabricated from a van der Waals epitaxially grown Bi_2Te_3 nanoplate directly on the growth mica substrate. The top-gate voltage dependent measurements of the sheet resistance reveal that the transport carriers in the nanoplate are of n-type. The measurements also show that with decreasing top-gate voltage V_g , the sheet resistance initially increases quickly at large positive V_g but then turns to exhibit a slower increase with decreasing V_g , indicating an enhanced Coulomb screening against the top gate by the gradually separated top surface-state electrons. The carrier density is found to decrease with decreasing V_g , but the mobility shows a continuous increase with decreasing V_g , implying a reduction in the surface-bulk inter-channel scattering at a lower V_g . The measured magnetoconductivity shows the WAL characteristics and is analyzed by taking electron scattering between the top surface and bulk states into account. The dephasing times, τ_{φ_1} and τ_{φ_2} , and diffusion coefficients, D_1 and D_2 , of electrons in the bulk and at the top surface, as well as the scattering time τ_{SB_1} for electron from the bulk to the top surface and the scattering time τ_{SB_2} for electron from the top surface to the bulk are extracted. It is shown that both τ_{φ_1} and τ_{φ_2} decrease with decreasing V_g . However, τ_{SB_1} is seen to increase with decreasing V_g , while τ_{SB_2} is found to be nearly independent of V_g . This result is explained by considering the characteristic difference in the density of states in the bulk and at the top surface. The diffusion coefficients D_1 and D_2 in the bulk and at the top surface are found to be top-gate voltage V_g -independent. This result, together with the observed decrease in τ_{φ_1} and τ_{φ_2} with decreasing V_g , leads to the observation that the dephasing lengths in the bulk L_{φ_1} and at the top surface L_{φ_2} are decreased with decreasing V_g , in agreement with the results reported in the literature. The measures of coherent coupling of the bulk and top-surface 2D channels, $\tau_{\varphi_1}/\tau_{\text{SB}_1}$ and $\tau_{\varphi_2}/\tau_{\text{SB}_2}$ are also extracted. It is found that both increase with increasing V_g and are > 1 at the considered values of V_g at $T = 2$ K, providing an evidence that the transport is in the top surface-bulk coherently coupled regime.

Temperature-dependent measurements of the magnetoconductivity in the top-gated Bi_2Te_3 nanoplate Hall-bar device are also performed at $V_g = -10$ V (a weak top surface-bulk coherently coupled case). It is found that for temperatures $T = 2$ K to 14 K, the diffusion coefficients, D_1 and D_2 , and the inter-channel scattering times, τ_{SB_1} and τ_{SB_2} , all show to be temperature independent. However, the dephasing times τ_{φ_1} and τ_{φ_2} , the dephasing lengths L_{φ_1} and L_{φ_2} , and the ratios $\tau_{\varphi_1}/\tau_{\text{SB}_1}$ and $\tau_{\varphi_2}/\tau_{\text{SB}_2}$ are all found to be decreased

with increasing temperature. Importantly, it is found that $L_{\varphi_1} \sim T^{-0.55}$ and $L_{\varphi_2} \sim T^{-0.49}$, showing that the electron dephasing is dominated by the electron-electron scattering with small energy transfers. In addition, $\tau_{\varphi_1}/\tau_{SB_1}$ is found to become < 1 at temperatures $T = 6$ K to 14 K. This result shows that the transport in the bulk can be treated as coherently decoupled from the top surface. However, $\tau_{\varphi_2}/\tau_{SB_2}$ is found to be > 1 at $T = 2$ K to 14 K, showing that the transport in our Bi_2Te_3 nanoplate cannot be strictly treated as coherent transport through fully decoupled top-surface and bulk 2D channels at these low temperatures. Our study presented in this work shows that it is important to consider surface-bulk state coupling explicitly when analyzing the magnetotransport in a 3D topological insulator nanoplate.

AUTHOR CONTRIBUTIONS

H. Q. Xu conceived and supervised the project. X. Li grew the material, fabricated the device and performed the transport measurements. X. Li and H. Q. Xu analyzed the measurement data. M. Meng and S. Huang participated in the device fabrication, the transport measurements, and the data analysis. C. Tan, C. Zhang and H. Peng participated in the material growth and performed the atomic force microscopy (AFM) measurements of the material. X. Li and H. Q. Xu wrote the manuscript with contributions from all the authors.

CONFLICTS OF INTEREST

There are no conflicts of interests to declare.

ACKNOWLEDGEMENTS

This work is supported by the Ministry of Science and Technology of China through the National Key Research and Development Program of China (Grant Nos. 2017YFA0303304, 2017YFA0204901, 2016YFA0300601, and 2016YFA0300802), the National Natural Science Foundation of China (Grant Nos. 92165208, 11874071, 91221202, 91421303, and 11974030), the Beijing Natural Science Foundation (Grant No. 1202010), and the Beijing Academy of Quantum Information Sciences (No. Y18G22).

REFERENCES

- ¹ M. Z. Hasan and C. L. Kane, *Rev. Mod. Phys.*, 2010, **82**, 3045.
- ² X. Qi and S. Zhang, *Rev. Mod. Phys.*, 2011, **83**, 1057.
- ³ A. Roth, C. Brüne, H. Buhmann, L. W Molenkamp, J. Maciejko, X. Qi, and S. Zhang, *Science*, 2009, **325**, 294.
- ⁴ D. Pesin and A. H. MacDonald, *Nature Mater.*, 2012, **11**, 409.
- ⁵ L. Fu and C. L. Kane, *Phys. Rev. Lett.*, 2008, **100**, 096407.
- ⁶ G. Bergmann, *Phys. Rep.*, 1984, **107**, 1.
- ⁷ H. He, G. Wang, T. Zhang, I. Sou, G. K. L Wong, J. Wang, H. Lu, S. Shen, and F. Zhang, *Phys. Rev. Lett.*, 2011, **106**, 166805.
- ⁸ A. A. Taskin, S. Sasaki, K. Segawa, and Y. Ando, *Phys. Rev. Lett.*, 2012, **109**, 066803.
- ⁹ M. Lang, L. He, X. Kou, P. Upadhyaya, Y. Fan, H. Chu, Y. Jiang, J. H. Bardarson, W. Jiang, E. S. Choi, Y. Wang, N. Yeh, J. Moore, and K. L. Wang, *Nano Lett.*, 2013, **13**, 48.
- ¹⁰ Y. S. Kim, M. Brahlek, N. Bansal, E. Edrey, G. A. Kapilevich, K. Iida, M. Tanimura, Y. Horibe, S. Cheong, and S. Oh, *Phys. Rev. B*, 2011, **84**, 073109.
- ¹¹ Z. Li, I. Garate, J. Pan, X. Wan, T. Chen, W. Ning, X. Zhang, F. Song, Y. Meng, X. Hong, X. Wang, L. Pi, X. Wang, B. Wang, S. Li, M. A. Reed, L. Glazman, and G. Wang, *Phys. Rev. B*, 2015, **91**, 041401(R).
- ¹² J. G. Checkelsky, Y. S. Hor, R. J. Cava, and N. P. Ong, *Phys. Rev. Lett.*, 2011, **106**, 196801.
- ¹³ J. Chen, X. Y. He, K. H. Wu, Z. Q. Ji, L. Lu, J. R. Shi, J. H. Smet, and Y. Q. Li, *Phys. Rev. B*, 2011, **83**, 241304(R).
- ¹⁴ J. Liao, Y. Ou, H. Liu, K. He, X. Ma, Q. Xue, and Y. Li, *Nat. Commun.*, 2017, **8**, 16071.
- ¹⁵ H. Steinberg, J. Laloë, V. Fatemi, J. S. Moodera, and P. Jarillo-Herrero, *Phys. Rev. B*, 2011, **84**, 233101.
- ¹⁶ S. Chiu and J. Lin, *Phys. Rev. B*, 2013, **87**, 035122.
- ¹⁷ L. Wang, Y. Yan, Z. Liao, and D. Yu, *Appl. Phys. Lett.*, 2015, **106**, 063103.
- ¹⁸ I. Garate and L. Glazman, *Phys. Rev. B*, 2012, **86**, 035422.
- ¹⁹ R. K. Gopal, S. Singh, A. Mandal, J. Sarkar, and C. Mitra, *Sci. Rep.*, 2017, **7**, 4924.
- ²⁰ H. Li, J. Cao, W. Zheng, Y. Chen, D. Wu, W. Dang, K. Wang, H. Peng, and Z. Liu, *J. Am. Chem. Soc.*, 2012, **134**, 6132.
- ²¹ X. Yu, L. He, M. Lang, W. Jiang, F. Xiu, Z. Liao, Y. Wang, X. Kou, P. Zhang, J. Tang, G. Huang, J. Zou, and K. L Wang, *Nanotechnology*, 2013, **24**, 015705.

- ²² A. Roy, S. Guchhait, S. Sonde, R. Dey, T. Pramanik, A. Rai, H. C. P. Movva, L. Colombo, and S. K. Banerjee, *Appl. Phys. Lett.*, 2013, **102**, 163118.
- ²³ Y. Jing, S. Huang, J. Wu, M. Meng, X. Li, Y. Zhou, H. Peng, and H. Xu, *Adv. Mater.*, 2019, **31**, 1903686.
- ²⁴ C. B. Satterthwaite and R. W. Ure Jr., *Phys. Rev.*, 1957, **108**, 1164.
- ²⁵ Y. L. Chen, J. G. Analytis, J. Chu, Z. K. Liu, S. Mo, X. L. Qi, H. J. Zhang, D. H. Lu, X. Dai, Z. Fang, S. C. Zhang, I. R. Fisher, Z. Hussain, and Z. Shen, *Science*, 2009, **325**, 178.
- ²⁶ S. Hikami, A. I. Larkin, and Y. Nagaoka, *Prog. Theor. Phys.*, 1980, **63**, 707.
- ²⁷ Y. Jing, S. Huang, K. Zhang, J. Wu, Y. Guo, H. Peng, Z. Liu, and H. Q. Xu, *Nanoscale*, 2016, **8**, 1879.
- ²⁸ Y. Ni, Z. Zhang, C. I. Nlebedim, and D. C. Jiles, *AIP Advances*, 2016, **6**, 055812.
- ²⁹ W. Mortelmans, S. D. Gendt, M. Heyns, and C. Merckling, *Appl. Mater. Today*, 2021, **22**, 100975.
- ³⁰ B. L. Altshuler, A. G. Aronov, and D. E. Khmel'nitsky, *J. Phys. C*, 1982, **15**, 7367.

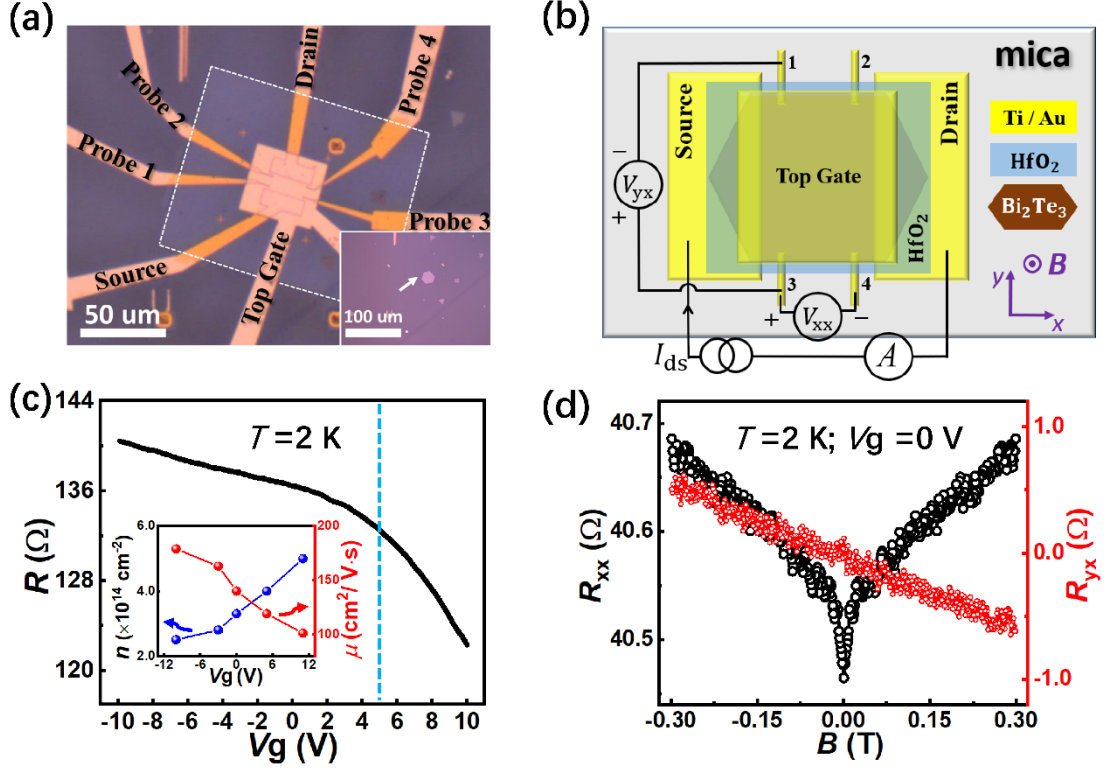


FIG. 1. (a) Optical image of the top-gated Hall-bar Bi_2Te_3 nanoplate device studied in this work. The inset shows an optical image of a few Bi_2Te_3 nanoplates grown on mica. The device is made from a ~ 12 -nm-thick, hexagonal nanoplate marked by the white arrow in the inset. (b) Schematic diagram of the device structure and the measurement circuit setup. (c) Measured sheet resistance R of the device vs. top-gate voltage V_g at $T = 2$ K. The blue vertical dashed line marks a top-gate voltage value of $V_g = 5$ V. Inset: measured sheet electron density n and Hall mobility μ vs. top-gate voltage V_g at $T = 2$ K. (d) Longitudinal resistance R_{xx} and Hall resistance R_{yx} of the device as a function of the magnetic field B at $T = 2$ K and $V_g = 0$ V. The magnetic field B is applied perpendicular to the substrate, as indicated in Fig 1(b).

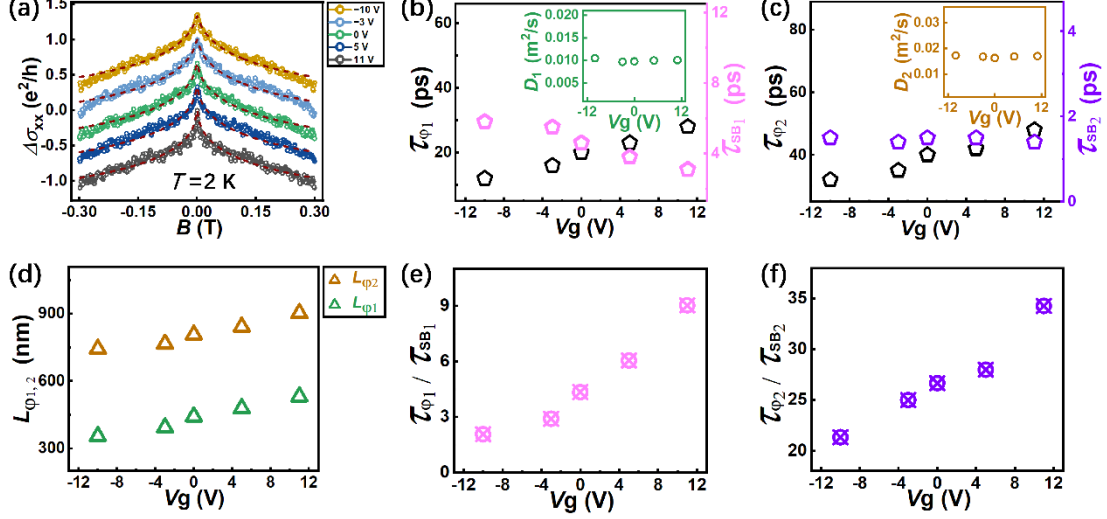


FIG. 2. (a) Magnetoconductivity $\Delta\sigma_{xx}$ of the device at different top gate voltages at $T = 2$ K. The opened circles show the measured data. The black ones are obtained at $V_g = 11$ V and the ones at other values of V_g are successively vertically offset for clarify. The dashed lines show the fits of the measured data using Eq (1). (b) Dephasing time τ_{ϕ_1} and bulk-to-surface scattering time τ_{SB_1} of electrons in the bulk vs. top-gate voltage V_g . Inset: diffusion coefficient D_1 of electrons in the bulk vs. top-gate voltage V_g . (c) Dephasing time τ_{ϕ_2} and surface-to-bulk scattering time τ_{SB_2} of electrons at the surface vs. top-gate voltage V_g . Inset: diffusion coefficient D_2 of electrons at the surface vs. top-gate voltage V_g . (d) Dephasing lengths L_{ϕ_1} and L_{ϕ_2} vs. top-gate voltage V_g . (e) $\tau_{\phi_1}/\tau_{SB_1}$ vs. top-gate voltage V_g . (f) $\tau_{\phi_2}/\tau_{SB_2}$ vs. top-gate voltage V_g .

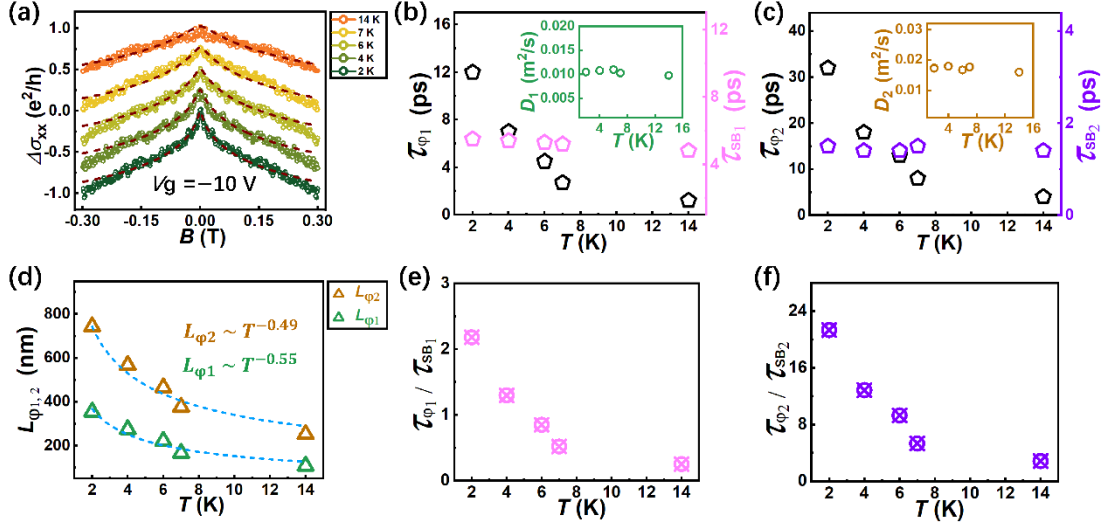


FIG. 3. (a) Magnetoconductivity $\Delta\sigma_{xx}$ of the device at different temperatures at $V_g = -10$ V. Again, the opened circles show the measured data. The dark green ones are obtained at temperature $T = 2$ K and the ones at other temperatures are successively vertically offset for clarify. The dashed lines show the fits of the measured data using Eq (1). (b) Dephasing time τ_{ϕ_1} and bulk-to-surface scattering time τ_{SB_1} of electrons in the bulk vs. temperature T . Inset: diffusion coefficient D_1 of electrons in the bulk vs. temperature T . (c) Dephasing time τ_{ϕ_2} and surface-to-bulk scattering time τ_{SB_2} of electrons at the surface vs. temperature T . Inset: diffusion coefficient D_2 of electrons at the surface vs. temperature T . (d) Dephasing lengths L_{ϕ_1} and L_{ϕ_2} vs. temperature T . Both L_{ϕ_1} and L_{ϕ_2} are found to exhibit a power-law temperature dependence as $L_{\phi_1} \sim T^{-0.55}$ and $L_{\phi_2} \sim T^{-0.49}$. (e) $\tau_{\phi_1}/\tau_{SB_1}$ vs. temperature T . (f) $\tau_{\phi_2}/\tau_{SB_2}$ vs. temperature T . Here, we note that $\tau_{\phi_2}/\tau_{SB_2} = 2.9$ at $T = 14$ K.